Arabian Journal of Chemistry (2020) 13, 5581–5592

King Saud University

Arabian Journal of Chemistry

www.ksu.edu.sa
www.sciencedirect.com

ORIGINAL ARTICLE

Spectroscopic investigation of $La_7Ta_3W_4O_{30}:Sm^{3+}$ orange-red phosphor for white LEDs

Yu Wang [a], Bin Deng [b,c,*], Yuee Ke [a], Shuang Shu [a], Rixin Liu [a], Ruijin Yu [a,*]

[a] College of Chemistry & Pharmacy, Northwest A&F University, Yangling, Shaanxi 712100, PR China
[b] College of Chemical Biological and Environmental Engineering, Xiangnan University, Chenzhou, Hunan 423043, PR China
[c] Hunan Provincial Key Laboratory of Xiangnan Rare-Precious Metals Compounds Research and Application, Chenzhou, Hunan 423043, PR China

Received 13 November 2019; accepted 22 March 2020
Available online 31 March 2020

KEYWORDS

Luminescence;
Tungstate;
$La_7Ta_3W_4O_{30}:Sm^{3+}$;
Phosphor

Abstract The novel orange-red light emitting $La_7Ta_3W_4O_{30}:xSm^{3+}$ (x = 0.005–0.20) phosphors were synthesized via the solid-state reaction method. The crystal structure, photoluminescence (PL) properties, optimum concentration, color purity, decay life, and thermal stability of the samples were systematically studied. Under the excitation of 404 nm, $La_7Ta_3W_4O_{30}:Sm^{3+}$ emits intense orange-red light at 597 nm. The PL spectra of $La_7Ta_3W_4O_{30}:Sm^{3+}$ phosphors are ascribed to the $^4G_{5/2}$ to ^6H_J (J = 5/2, 7/2, 9/2, and 11/2) transitions of Sm^{3+} ions. The concentration quenching occurs at the doping level of 1 mol%. The quenching temperature is higher than 500 K. Finally, a white LED (w-LED) with the Commission Internationale de L'Eclairage (CIE) chromaticity coordinates of (0.312, 0.296) and good color rendering index (Ra) of 86 was fabricated. As a consequence, all the results suggest that the orange-red phosphors $La_7Ta_3W_4O_{30}:Sm^{3+}$ have potential applications in w-LEDs structures.

1. Introduction

At present, w-LEDs, as new ideal lighting sources, rapidly substitute the traditional fluorescent and incandescent lamps owing to its excellent advantages, such as environment-friendly, lower power consumption, robustness, durability, long operation time, high brightness and small size (Cao et al., 2019; Xu et al., 2013; Zhao et al., 2017; Min et al., 2017). Currently, the major way to manufacture w-LEDs is to merge the InGaN blue-emitting chip with yellow phosphor $Y_3Al_5O_{12}:Ce^{3+}$ (YAG) (Tang et al., 2017; Atuchin et al., 2015; Ji et al., 2016; Galashov et al., 2017). Nonetheless, this product has some drawbacks, such as the high correlated color temperature (CCT) and low Ra, and these shortcomings make it dif-

* Corresponding authors at: College of Chemical Biological and Environmental Engineering, Xiangnan University, Chenzhou, Hunan 423043, PR China (B. Deng).
E-mail addresses: ddhbyjs@126.com (B. Deng), yuruijin@nwsuaf.edu.cn (R. Yu).
Peer review under responsibility of King Saud University.

Production and hosting by Elsevier

https://doi.org/10.1016/j.arabjc.2020.03.018
1878-5352

ficult to develop the w-LEDs in the future (Wang et al., 2019). To resolve these problems, red-emitting phosphors can be applied to decrease CCT and improve the Ra value. As to commercial red phosphors of $YVO_4:Eu^{3+}$, $Y_2O_2S:Eu^{3+}$ and $Y_2O_3:Eu^{3+}$, they absorb insufficiently in the NUV (near ultraviolet) region (Tang et al., 2014; Guo et al., 2008; Al-Mamun and Ishigaki, 2014). For some red nitride phosphors, such as $CaAlSiN_3:Eu^{2+}$, $Sr_2Si_5N_8:Eu^{2+}$, and $Sr_xCa_{1-x}AlSiN_3:Eu^{2+}$, the high pressure and high temperature conditions are needed for synthetic (Li et al., 2015; Wang et al., 2018; Zou et al., 2016). Hence, in w-LEDs production, it is significant to investigate new red phosphors.

In a large number of rare-earth ions doped phosphors, Sm^{3+} ions are considered to be among the most popular and effective doped ions due to its outstanding luminescence properties. Sm^{3+} ions exhibit intensity emission in reddish orange region due to its $^4G_{5/2} \rightarrow {}^6H_J$ (J = 5/2, 7/2, 9/2, and 11/2) transitions in such phosphors $Sr_2MgTeO_6:Sm^{3+}$, $LiCa_3MgV_3O_{12}:Sm^{3+}$ and $Y_{1-x-y}Gd_xVO_4:ySm^{3+}$ (Zhao et al., 2019; Huang and Guo, 2018; Jaiswal et al., 2020).

In a general way, the selection of appropriate host materials are particularly significant for efficient luminescence of rare-earth ions. Rare-earth tungstates demonstrate high thermal and chemical stability, have good absorption in the NUV region and widely used in laser technology (Zhang et al., 2016; Atuchin et al., 2008, 2005). Hence, the preparation and properties of tungstate doped rare earth luminescent materials have aroused more and more interests. For instance, $Y_6WO_{12}:Dy^{3+}$, $Lu_{2-x}Sm_xWO_6$ and $KLaMgWO_6:Mn^{4+}$ can be pointed (Yu et al., 2014; Zhang et al., 2018; Liang et al., 2019). Recently, the columnar-perovskite-type $La_7W_4M_3O_{30}$ (M = Nb, Ta) tungstate has been found to be a member of the $A_7B_7O_{30}$ (A = La, B = Mo) family (Lacorre and Corbel, 2019). However, up to now, there were no reports on the optical properties of Sm^{3+} ions doped in $La_7Ta_3W_4O_{30}$ tungstate phosphor.

In this work, the novel orange-red emitting $La_7Ta_3W_4O_{30}:xSm^{3+}$ (LTWO:xSm^{3+}) phosphors were synthesized. The structural characterization, PL excitation (PLE) and PL properties, optimum concentrations, thermal stability and CIE chromaticity coordinates of the LTWO:xSm^{3+} phosphors were studied systematically. At final, a white LED with good Ra was fabricated by using LTWO:$0.01Sm^{3+}$ phosphor.

2. Experimental procedure

2.1. Preparation

LTWO:xSm^{3+} (x = 0.005, 0.01, 0.02, 0.05, 0.10, 0.15 and 0.20) phosphors were prepared by the method of solid-state synthesis method. The raw materials were La_2O_3 (99.99%), WO_3 (99.8%), Ta_2O_5 (99.5%), and Sm_2O_3 (99.99%), which were from Sigma-Aldrich. The powder was weighed on the basis of the stoichiometric ratio and then ground appropriately in an agate mortar. Then, the mixtures were preheated at 700 °C for 2 h in the air, then reground and sintered at 1350 °C for 10 h in the air. Eventually, the phosphor powders of white color were obtained. The equation for this reaction is as follows:

$$7(1-x)La_2O_3 + 8WO_3 + 3Ta_2O_5 + 7xSm_2O_3 \rightarrow 2La_{7(1-x)}Sm_{7x}Ta_3W_4O_{30}$$

2.2. Measurements

The X-ray diffraction (XRD) patterns were recorded by a Bruker D2 PHASER X-ray diffractometer with use of Cu Kα radiation (λ = 0.15405 nm) in the 2θ angle range of 10° to 70°. The morphology of LTWO:Sm^{3+} samples was measured by a Nova Nano SEM-450 field emission scanning electron microscopy (SEM). The size distribution was examined by a Malvern MS2000 laser particle size analyzer. The PL spectra at different temperatures (300–500 K) and the decay times were studied with the use of an Edinburgh FLS 980 spectrometer. The electroluminescence spectrum (EL) of the w-LED fabricated with LTWO:Sm^{3+} phosphor was examined by a fiber optic spectrometer Ocean Optics, USB 4000.

3. Results and discussion

3.1. Phase analysis

Fig. 1 (a) is the crystal structure of LTWO, which belongs to the trigonal crystal system, with R-3 (No.148) space group. The cell parameters are $a = b = 17.0701(2)$ Å, $c = 6.8851(1)$ Å, $V = 1737.45(5)$ Å^3, and $Z = 3$ (Goutenoire et al., 2005; La7Ta3W4O30 Crystal Structure). The new compound LTWO has the same structure type as $La_7Mo_7O_{30}$ and it belongs to the $A_7B_7O_{30}$ family. This type is a columnar-perovskite-type arrangement, which is formed by the isolated hexagonal perovskite building units (Goutenoire et al., 1999). In this structure, the 3b site is occupied by Ta(1), it coordinated with six oxygen atoms, and all the Ta(1)-O distances are equal to 1.9922 Å but the bond angles are different. Thus, the coordination polyhedron [Ta(1)O_6] is an almost regular octahedron as shown in Fig. 1 (b). The coordination of Ta (2)/W(1) is similar to Ta(1), and the coordination polyhedron [Ta(2)/W(1)O_6] is also an octahedron with six oxygen atoms, but with a strong distortion, the bond length is between 1.8824 and 2.2401 Å. The coordination polyhedron of La(1) and La(2) are different. La(1) occupies the 3a site which coordinates with twelve oxygen atoms and the coordination polyhedron [La(1)O_{12}] is a quasi-normal icosahedron with La-O distances ranging from 2.5619 to 2.7318 Å. La(2) is coordinated with nine oxygen atoms, and the coordination polyhedron [La(2)O_9] is more distorted, with the minimum bond length of 2.4231 Å^3 and the maximum bond length of 2.8605 Å. The atom coordinates in LTWO structure are listed in Table 1. Moreover, with the purpose of further studying the substituted ions (La^{3+}) in LTWO host lattices, the result can be estimated by this equation (Sun et al., 2018):

$$D_r = \frac{R_1(CN) - R_2(CN)}{R_1(CN)} \times 100\% \quad (1)$$

In this equation, D_r is the radius percentage difference, R_1 and R_2 are the radius of the substituted ions and doped ions, respectively. CN is the coordination number. In this work, Sm^{3+} ions can replace La(1) and La(2), the coordination numbers are 12 and 9, respectively. When CN = 12, the radius of La(1) and Sm^{3+} ions are 1.032 Å and 0.958 Å, the D_r value is equal to 7.17% (Shannon, 1976). When CN = 9, the radius of La(2) and Sm^{3+} ions are 1.1 Å and 1.02 Å, the value of D_r is 7.27%. In both cases, the Dr Values are less than 30%, indicat-

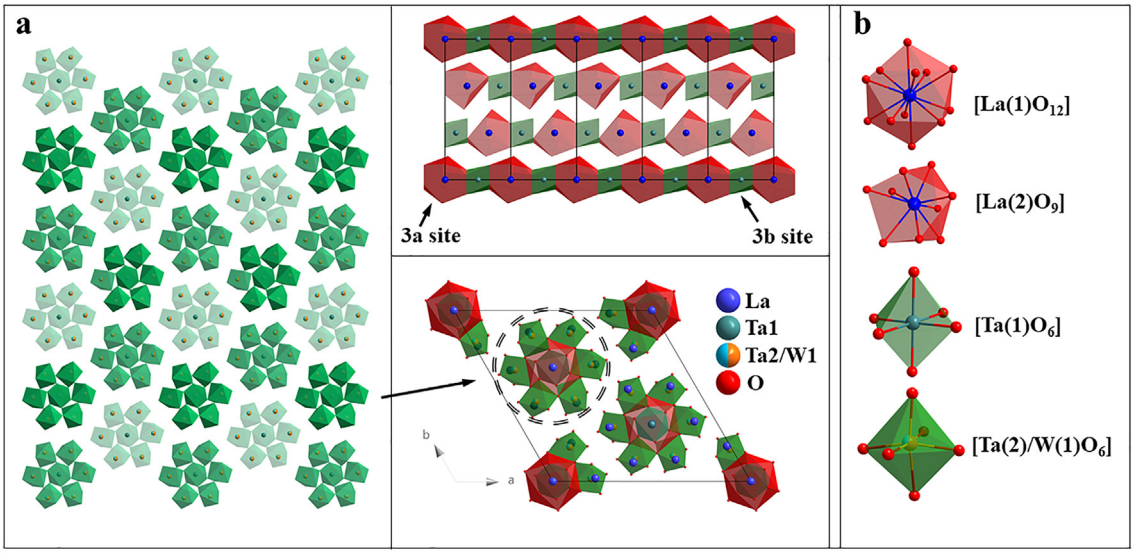

Fig. 1 (a) The crystal structure of LTWO. (b) The coordination environment of La(1), La(2), Ta(1) and Ta(2)/ W(1) atoms.

Table 1 The crystal parameter of LTWO.

Atom	Site	Occupancy	*x*	*y*	*z*
La1	3a	1	0	0	0
Ta1	3b	1	0	0	0.5
La2	18f	1	0.7766(2)	−0.0173(2)	0.3443(4)
W1/Ta2	18f	0.66/0.33	0.1998(2)	0.0151(2)	0.1596(5)
O1	18f	1	0.2460(2)	0.1006(2)	0.3563(5)
O2	18f	1	0.2930(2)	0.0431(2)	−0.0074(5)
O3	18f	1	0.1691(2)	0.1118(2)	0.0454(5)
O4	18f	1	0.2044(3)	−0.0726(2)	0.3067(4)
O5	18f	1	0.0348(2)	0.1049(2)	0.3237(5)

ing that Sm^{3+} ions can replace La^{3+} ions without damaging the crystal structure, and the D_r value of La(1) is less than that of La(2), manifesting that Sm^{3+} ions occupy La(1) site first.

The XRD patterns of LTWO:$x$$Sm^{3+}$ (x = 0.005–0.20) phosphors are shown in Fig. 2 (a). The simulated pattern for LTWO host is obtained according to the study of F. Goute-

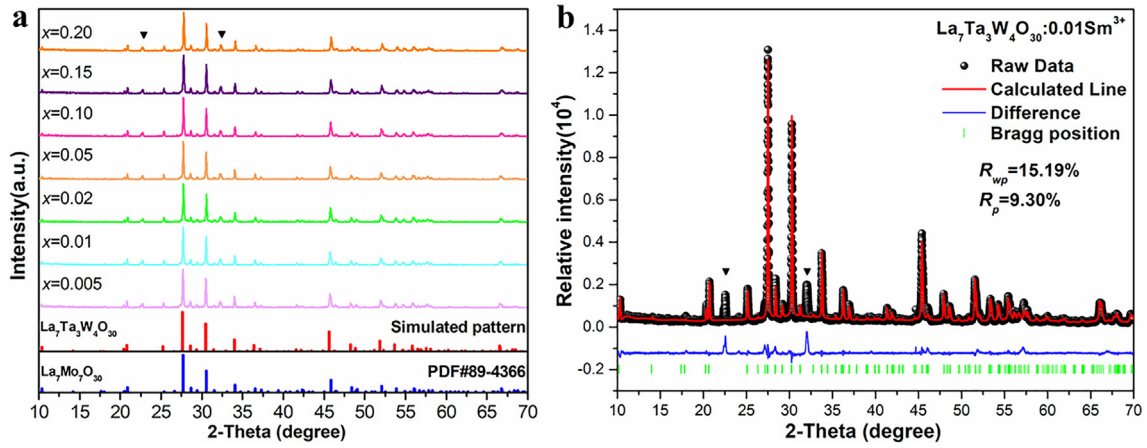

Fig. 2 (a) The XRD patterns of LTWO:$x$$Sm^{3+}$ (x = 0.005–0.20) phosphors. (b) The Rietveld refinement of the LTWO:0.01Sm^{3+} phosphor.

noire et al. (Goutenoire et al., 2005). By comparison, it is clearly that the peaks of all samples fit well with the simulated pattern of LTWO. It also matches well with the $La_7Mo_7O_{30}$ standard card (PDF 89-4366), which indicated that the structure of LTWO is the same as $La_7Mo_7O_{30}$. But there are two small impure peaks in the XRD patterns, which are ascribed to $La_{0.33}TaO_3$ admixture (PDF 42-0061) (Trunov et al., 1968). Therefore, the experimental conditions will be further optimized. For the purpose of further studying the Sm^{3+} environment, the Rietveld refinement of the LTWO:0.01Sm^{3+} phosphor by GSAS software was carried out and the different pattern is presented in Fig. 2(b). As obtained by Rietveld analysis, the LTWO:0.01Sm^{3+} compound crystallized with unit cell parameters of $a = b = 17.1125$ Å, $c = 6.9177$ Å, $V = 1754.376$ Å^3, and $Z = 3$ ($R_{wp} = 15.19\%$, $R_p = 9.30\%$). The appropriate R_{wp} and R_p values indicate that the Sm^{3+} ions have successfully replaced La^{3+} ions. Furthermore, the refinement parameters of the sample are listed in Table 2.

The particle sizes and surface morphology are significant for the phosphor properties. The SEM micrographs of the samples with doping concentrations of 2 and 20 mol%, which are monitored at the magnification of 20,000 times are shown in Fig. 3(a) and (b), respectively. It is obvious that the samples are mainly composed of partly coalescent particles and the particle diameters are very small and evenly distributed. It could be mentioned that such particle morphology is formed due to intense grain interdiffusion and it is typically observed in oxide compounds subjected to high temperature treatment (Atuchin et al., 2008; Lim et al., 2015). Comparing the panels, it can be concluded that the Sm^{3+} ion concentration has little effect on the particle size. The particle size distribution in LTWO:0.20Sm^{3+} is presented in Fig. 3(c). The highest peak value of the particle size distribution is 21.678 μm, indicating the particle size of samples is mainly distributed around 21 μm. Therefore, this sample has the potential to be used in industrial w-LEDs.

In Fig. 4, the optical band gap (E_g) determination in the LTWO and LTWO:0.01Sm^{3+} compounds is shown. The samples have a strong absorption between 200 and 350 nm. Based on the relation between $(\alpha hv)^2$ and hv, the E_g value can be obtained by this formula (Devi et al., 2019):

$$(\alpha hv)^{1/n} = A(hv - Eg) \quad (2)$$

Table 2 The Refinement parameters of the LTWO:0.01Sm^{3+} phosphor.

Formula	$La_7Ta_3W_4O_{30}$:0.01Sm^{3+}
Space group	*R*-3 (No.148)
Cell parameters	$a = 17.1125$ Å
	$b = 17.1125$ Å
	$c = 6.9177$ Å
	$\alpha = \beta = 90°$
	$\gamma = 120°$
	$Z = 3$
Cell Volume (Å)	1754.376
χ^2	7.818
R_{wp}	15.19%
R_p	9.30%

where α is the absorption coefficient, hv means the photon energy, A is constant and n = 0.5 for direct transition. The E_g values of LTWO and LTWO:0.01Sm^{3+} are 3.44 and 3.38 eV, respectively.

3.2. Optical properties

The excitation spectrum of LTWO:0.01Sm^{3+}, as monitored at 597 nm at room temperature, is shown in Fig. 5. It is mainly composed of two components. The first component is a broad band of CTB (charge transfer band) between 200 and 350 nm. By Gaussian fitting, it is be found that the wide band consists of two broads (a) and (b), which are due to the electron transition of O^{2-}-Sm^{3+} and O^{2-}-W^{6+}, respectively (Li et al., 2017, 2011). The second component is a set of several sharp peaks appeared between 350 and 500 nm by the 4f-4f transitions of Sm^{3+} ions, which from the ground state $^6H_{5/2}$ to the excited states $^4D_{3/2}$, $^4D_{1/2}$, $^4F_{7/2}$, $(^6P,^4P)_{5/2}$, $^4G_{9/2}$, $^4I_{13/2}$ and $^4I_{11/2}$ at 361, 376, 404, 419, 439, 463 and 480 nm, respectively (Deng et al., 2015). Among these peaks, the highest one is located at 404 nm, manifesting that the samples can sufficiently be excited by the NUV chips and have a potential in w-LED manufacturing.

In Fig. 6(a), the emission spectrum is shown for LTWO:0.01Sm^{3+} phosphor excited at 404 nm, which revealed four obvious peaks between 500 and 750 nm. Distinctly, the peak at 597 nm, owing to $^4G_{5/2} \rightarrow {}^6H_{7/2}$ transition, has the highest intensity. Simultaneously, other characteristic peaks are centered at 561, 644 and 703 nm, which are in line with the 4f-4f electronic forbidden transitions of Sm^{3+} ions from the $^4G_{5/2}$ level to ^6H_J ($J = 5/2$, 9/2 and 11/2) levels (Guo et al., 2017; Atuchin et al., 2015, 2017). Among these peaks, the first peak at 561 nm is of MD (magnetic-dipole) natured, and the highest peak at 597 nm is combined MD and ED (electric-dipole) transition. The third peak at 644 nm is due to ED transition, which is sensitive to the crystal field. Based on Judd–Ofelt theory, the comparison of ED/MD ratio is a good way to judge the environment around the Sm^{3+} ions in LTWO host. The stronger the ED transition, the greater the asymmetry property, and vice versa. In this study, the ED transition (644 nm) is significantly stronger than the MD transition (561 nm) that indicates the asymmetry nature of Sm^{3+} ions in LTWO lattice. In Fig. 6(b), the Sm^{3+} energy level diagram, illustrating the Sm^{3+} ions energy transfer process in the LTWO host lattice, is given. Under the 404 nm excitation, Sm^{3+} ions at $^6H_{5/2}$ ground state level absorb photon energy, and the electrons excite to $^4F_{7/2}$ level, and, then the electrons of Sm^{3+} ions relax without radiation to the $^4G_{5/2}$ level. At final, the radiative transition of Sm^{3+} ions from $^4G_{5/2}$ level to ^6H_J (J = 5/2, 7/2, 9/2 and 11/2) levels are corresponding to four sharp peaks at 561, 597, 644 and 703 nm, respectively.

The emission spectra of LTWO:$x$$Sm^{3+}$ ($x = 0.005$–0.20) phosphors are shown in Fig. 7(a). It is evident that the characteristic peaks of all phosphors are of similar shape except for the intensity, and no wavelength shift is detected at high dopant concentrations. With the doping level increases, the emission intensity first increases. When the doping content is higher than 1%, the emission intensity gradually decreases owing to concentration quenching, as shown in the upper right corner of Fig. 7(a). The luminescence intensity quenching is resulted from the energy transfer between activators. The crit-

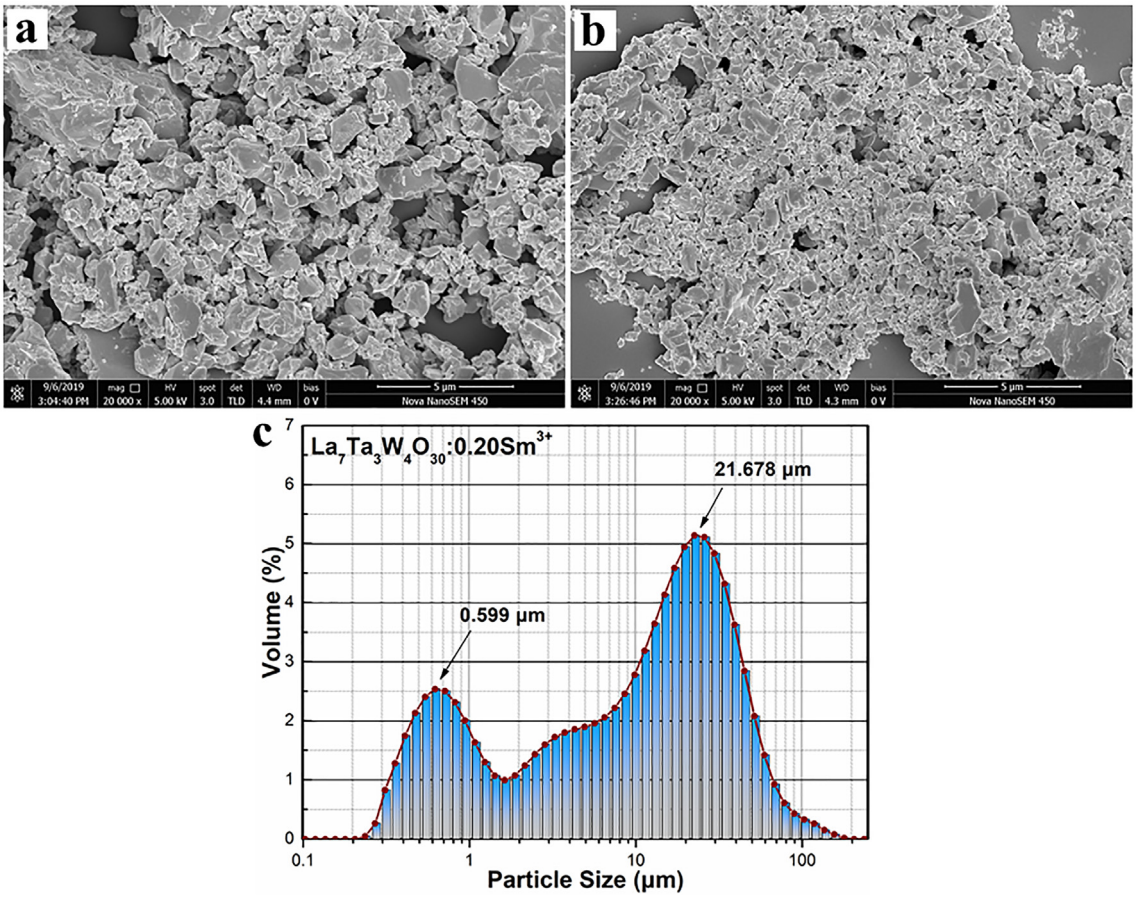

Fig. 3 (a) and (b) The SEM micrographs of LTWO:0.01Sm^{3+} and LTWO:0.20Sm^{3+}. (c) The particle size distribution of LTWO:0.20Sm^{3+}.

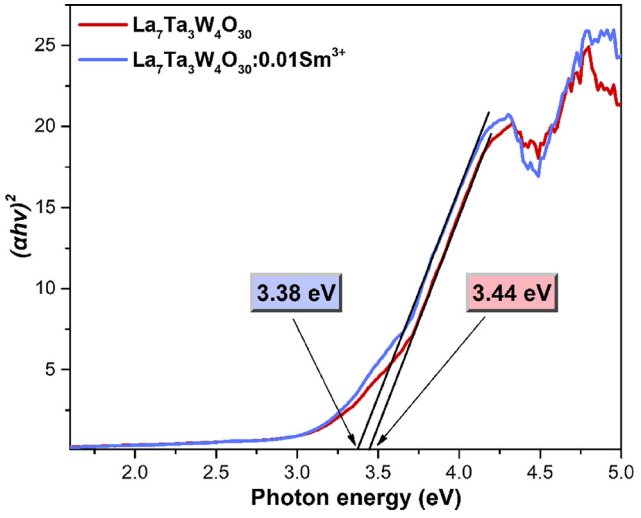

Fig. 4 The relationship between the $(\alpha h\nu)^2$ and photon energy for LTWO and LTWO:0.01Sm^{3+}.

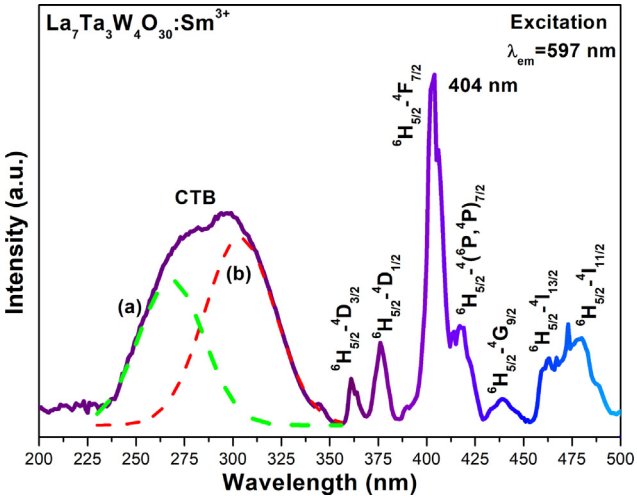

Fig. 5 Excitation spectrum of LTWO:0.01Sm^{3+} (λ_{em} = 597 nm).

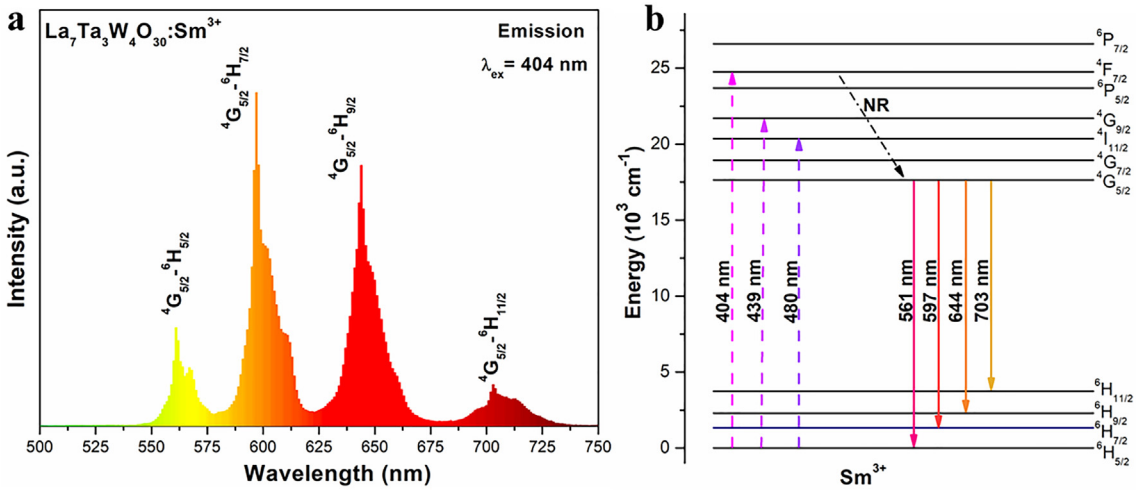

Fig. 6 (a) Emission spectrum of LTWO:0.01Sm^{3+} (λ_{ex} = 404 nm). (b) The Sm^{3+} energy level diagram.

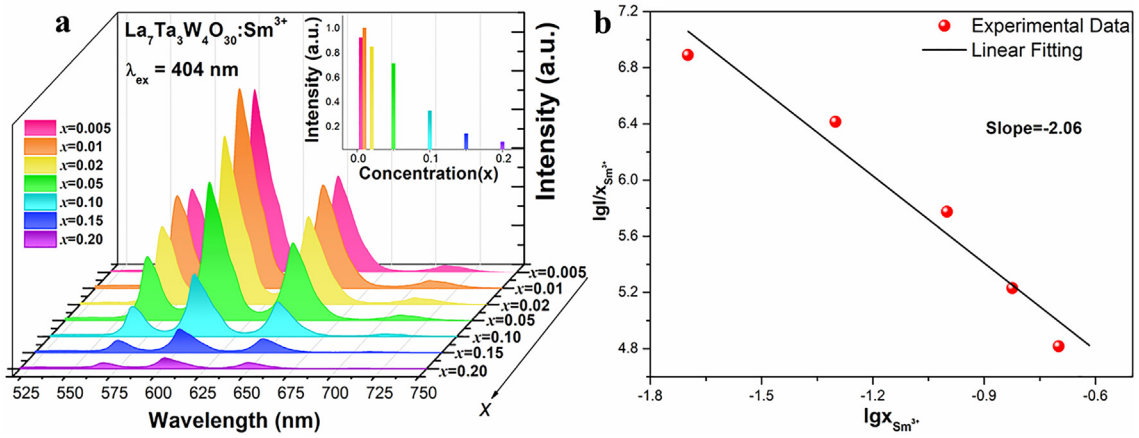

Fig. 7 (a) Emission spectra of several LTWO:$x$$Sm^{3+}$ (x = 0.005–0.20) phosphors (λ_{ex} = 404 nm). (Inset: The normalized intensity of the emission spectra). (b) The lg$I/x \sim$ lg$x$ diagram of LTWO:$x$$Sm^{3+}$ (x = 0.005–0.20) phosphors.

ical transfer distance (R_c) can be calculated by this formula (Xia and Liu, 2012):

$$R_c \approx 2\left(\frac{3V}{4\pi x_c N}\right)^{1/3} \tag{3}$$

where x_c stands the optimum concentration, N means the number of substitutable ions, V points the cell volume. In this work, V = 1754.376 Å^3, x_c = 0.01 and N = 3, and the value of R_c is equal to 48 Å. This result is greater than 5 Å, indicating that the main cause of concentration quenching is the multipole-multipole interaction.

Based on the theory of Dexter, the multipole interaction can be judged by the change of emission intensity (I) between the emission level and the multipole interaction. The value of I can be obtained by this equation (Chen et al., 2016):

$$\frac{I}{x} = K\left[1+\beta(x)^{Q/3}\right]^{-1} \tag{4}$$

where x points the doping concentration of Sm^{3+} ions, β and K are constants. Q value is controlled by the mechanism of dipole-dipole (6), dipole-quadrupole (8) or quadrupole-quadrupole (10) interaction. The multipole interaction can also be judged by this equation (Tian et al., 2011):

$$log\left(\frac{I}{x}\right) = A - \frac{Q}{3}log(x),\ \ A = log(K) - log(\beta) \tag{5}$$

The relation between lgI/x and lg$x$ of LTWO:Sm^{3+} phosphors is displayed in Fig. 7(b), which indicates that the slope of lgI/x to lg$x$ is −2.06. Afterward, Q is equal to 6.18, which is close to 6. This result manifests that the dipole-dipole interaction is the main mechanism of concentration quenching of Sm^{3+} ions emission in LTWO host.

3.3. CIE chromaticity coordinate and color purity

The CIE color coordinates of LTWO:$x$$Sm^{3+}$ (x = 0.005–0.20) phosphors can be calculated on the basis of PL spectra, and the formula is as follows (Robertson, 1968):

$$\begin{cases} X = \int_{500}^{750} P(\lambda)\,\bar{x}\,(\lambda)d\lambda \\ Y = \int_{500}^{750} P(\lambda)\,\bar{y}\,(\lambda)d\lambda \\ Z = \int_{500}^{750} P(\lambda)\,\bar{z}\,(\lambda)d\lambda \end{cases} \tag{6}$$

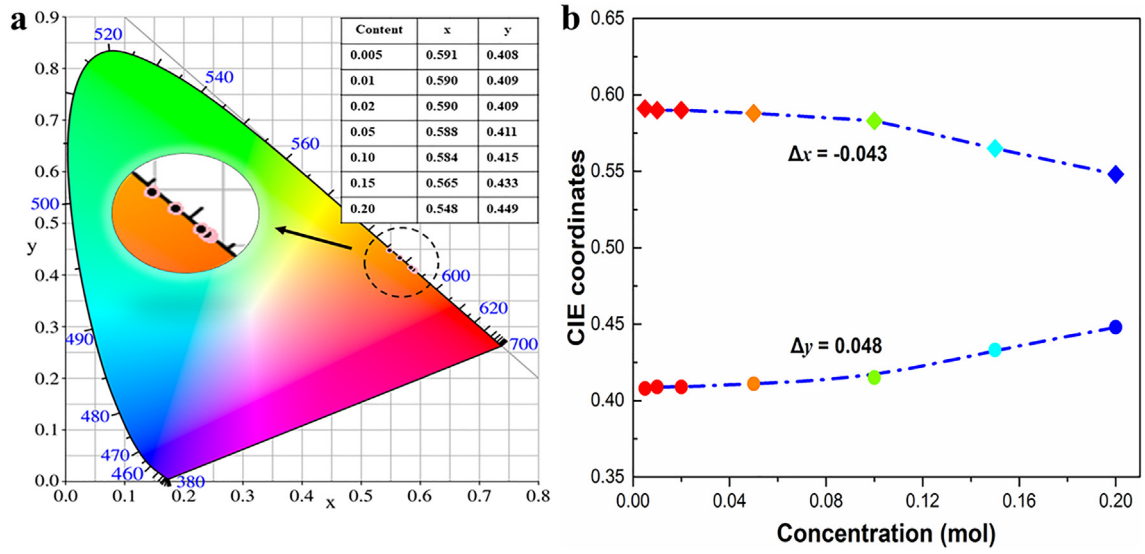

Fig. 8 (a) The CIE chromaticity graph of LTWO:xSm^{3+} (x = 0.005–0.20) phosphor. (b) The movement of color coordinates x and y of LTWO:xSm^{3+} (x = 0.005–0.20).

(In this study, the integral is obtained by summing in the range of 500–750 nm with the unit of 1 nm). Where X, Y, and Z are the tristimulus values that can be acquired from the $P(\lambda)$. $P(\lambda)$ means the PL spectral intensity at wavelength λ. $\bar{x}$, $\bar{y}$, and $\bar{z}$ are the color-matching functions. The CIE color coordinates of LTWO:Sm^{3+} phosphors are shown in Fig. 8(a). It is clear that all the coordinate points of phosphors are located at the boundary of the CIE graph, suggesting the samples have good color purity. Furthermore, the color purity can be calculated by this formula (Seeta Rama Raju et al., 2011):

$$\text{Color purity} = \frac{\sqrt{(x_s - x_i)^2 + (y_s - y_i)^2}}{\sqrt{(x_d - x_i)^2 + (y_d - y_i)^2}} \times 100\% \quad (7)$$

In this equation, (x_i, y_i) are the color coordinates of the optical source point (0.333, 0.333). (x_s, y_s) are the color coordinates value of the phosphor. (x_d, y_d) are the CIE color coordinates of the extension of the line that connects (x_s, y_s) to (x_i, y_i) to the boundary. For the LTWO:0.01Sm^{3+} phosphor, (x_s, y_s) are (0.590, 0.409),(x_d, y_d) are (0.590, 0.410). The obtained color purity is 99.9% by fitting the formula. The color purity and the CIE color coordinates of other doping concentrations are given in Table 3. In Fig. 8(b), the extension of Fig. 8(a) is shown, reflecting the color coordinates movement of LTWO:xSm^{3+} (x = 0.005–0.20) phosphors. In the process of gradually increasing the doping concentration, the x-coordinate shift is $\Delta x = -0.043$ and the y-coordinate shift is $\Delta y = 0.048$. The Δx and Δy values are small, indicating that the color purity is less affected by Sm^{3+} doping concentration. Therefore, the LTWO:Sm^{3+} phosphors have a potential to replace the common red phosphors in the w-LEDs application.

Table 3 The color purity and the CIE color coordinates of LTWO:xSm^{3+} (x = 0.005–0.20) phosphors.

Concentration × (mol)	CIE (x, y)	Color purity
0.005	(0.591, 0.408)	99.9%
0.01	(0.590, 0.409)	99.9%
0.02	(0.590, 0.409)	99.9%
0.05	(0.588, 0.411)	99.9%
0.10	(0.584, 0.415)	99.9%
0.15	(0.565, 0.433)	99.6%
0.20	(0.548, 0.449)	99.3%

3.4. Luminescence decay curves

The decay curves of LTWO:xSm^{3+} (x = 0.005, 0.01, and 0.02) phosphors, which are monitored at 597 nm and excited under 404 nm, are shown in Fig. 9. The decay curves can be well fitted by this formula (Huang et al., 2018):

$$I(t) = I0 + Aexp\left(\frac{-t}{\tau}\right) \quad (8)$$

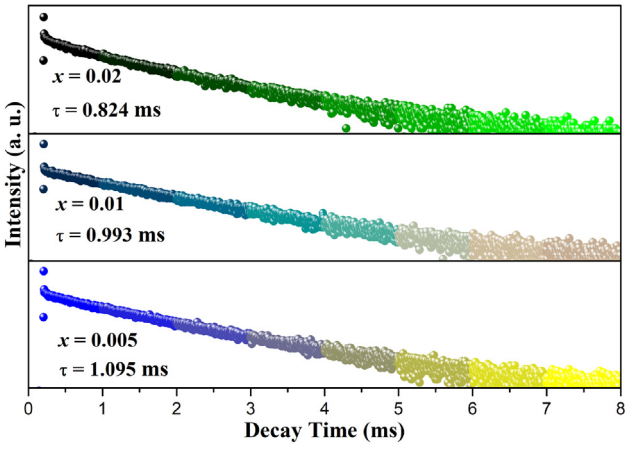

Fig. 9 The decay curves of LTWO:xSm^{3+} (x = 0.005, 0.01, and 0.02) phosphors.

In this equation, $I(t)$ is the luminescence intensity at time t. I_0 is system noise which exactly is the background of the fluorescence intensity (Zhang et al., 2018). A is a constant and τ is the decay lifetime. When the Sm^{3+} ions contents are 0.5; 1 and 2 mol%, the lifetime of Sm^{3+} ions in LTWO samples are 1.095, 0.993, and 0.824 ms, respectively. With the increase of doped Sm^{3+} ions, the critical distance decreases gradually, which makes the decay time shorten gradually.

3.5. Thermal stability

The phosphor thermal stability is an essential factor for w-LEDs application. Good phosphors are required to have good thermal stability to avoid thermal quenching at high temperature. The PL spectra of LTWO:0.01Sm^{3+} recorded from 300 to 500 K under 404 nm excitation are presented in Fig. 10(a). It is clear that all spectra have the same peak shape and position. With the temperature increase, the emission intensity of the phosphor decreases gradually. The emission intensity of the sample is 85% of the initial intensity at normal working temperature (420 K) of LED. $T_{0.5}$ is the quenching temperature while the emission intensity reduced to 50% of the initial intensity. It can be observed from the inset in Fig. 10 (a) that the $T_{0.5}$ of LTWO:0.01Sm^{3+} phosphor is greater than 500 K and the luminescence intensity decreased slightly. In Fig. 10 (b), the contour map of the strongest emission peak changing with temperature is shown. With the temperature increasing, the intensity of the emission peak at 597 nm decreases slowly.

The activation energy (E_a) of LTWO:Sm^{3+} can be obtained by the Arrhenius formula (Qiao et al., 2019):

$$I(T) = \frac{I_0}{1 + c\exp(-E_a/kT)} \quad (9)$$

where $I(T)$ represents the Sm^{3+} ions emission intensity at temperature T, I_0 is the initial luminescence intensity, c is a constant, and k is the Boltzmann constant (8.62×10^{-5} eV/K) (Tian et al., 2013). The relation of $\ln[(I_0/I)^{-1}]$ on $1/T$ is shown in Fig. 11 (a), and the E_a is determined to 0.28 eV. The thermal quenching mechanism of LTWO:Sm^{3+} phosphors is presented in Fig. 11 (b). Under the excitation of 404 nm, the electron transitions from the $^6H_{5/2}$ ground state to the $^4F_{7/2}$ excited state, afterward decreasing to the $^4G_{5/2}$ level without radiation (process ①), and then returns to the ground state through the radiation transition. As the temperature increases, some electrons at the $^4G_{5/2}$ level overcome the barrier of E_a through phonon-electron coupling to reach the junction between the $^4G_{5/2}$ level and CTB (process ②). Subsequently, these electrons will supply to CTB and relax to the $^6H_{5/2}$ ground state without radiation (process ③). The higher the temperature, the more electrons overcome the E_a to reach the junction, afterward the emission peak intensity of Sm^{3+} ion decreases gradually and the thermal quenching occurs. Furthermore, the LTWO:Sm^{3+} phosphors have a higher E_a (0.28 eV) comparing with those of $Ba_2Y_3(SiO_4)_3F:Sm^{3+}$ (0.13 eV) and $Li_3Gd_{2.85}Te_2O_{12}:Eu^{3+}$ (0.22 eV), and, so it has good thermal stability (Yu et al., 2015; Deng et al., 2017). All the results demonstrate that the LTWO:Sm^{3+} phosphors have wonderful thermal stability and good potential to be applied in w-LEDs manufacturing.

3.6. Fabrication of w-LED

For the purpose of investigating the application of LTWO:Sm^{3+} phosphors, a w-LED was fabricated by merging a NUV 407 nm chip with $BaMgAl_{10}O_{17}:Eu^{2+}$ (BAM, blue phosphor), $(Ba, Sr)_2SiO_4:Eu^{2+}$ (green phosphor) and the synthesized LTWO:0.01Sm^{3+} (orange-red phosphor). The EL spectrum of the w-LED is shown in Fig. 12(a). Several main peaks of the w-LED are located at 560, 595, 641, and 702 nm, which are basically consistent with previous spectroscopic data. The fabricated w-LED has high Ra (86) and good CCT (6818 K) that are comparable with the parameters of those of w-LED structures based on different phosphors (Xia et al., 2013; Ji et al., 2014; Leaño et al., 2016). Ra plays an important role in the application of w-LEDs, which is the average value of the special color rendering index from R1 to R8. R9 is the saturated red special color rendering index. R1 to R14 are special color rendering indexes, representing the color rendering performance of different colors (Wang et al., 2017). Fig. 12(b), the Ra value histogram is given for the fabricated w-LED and the commercial w-LED (blue

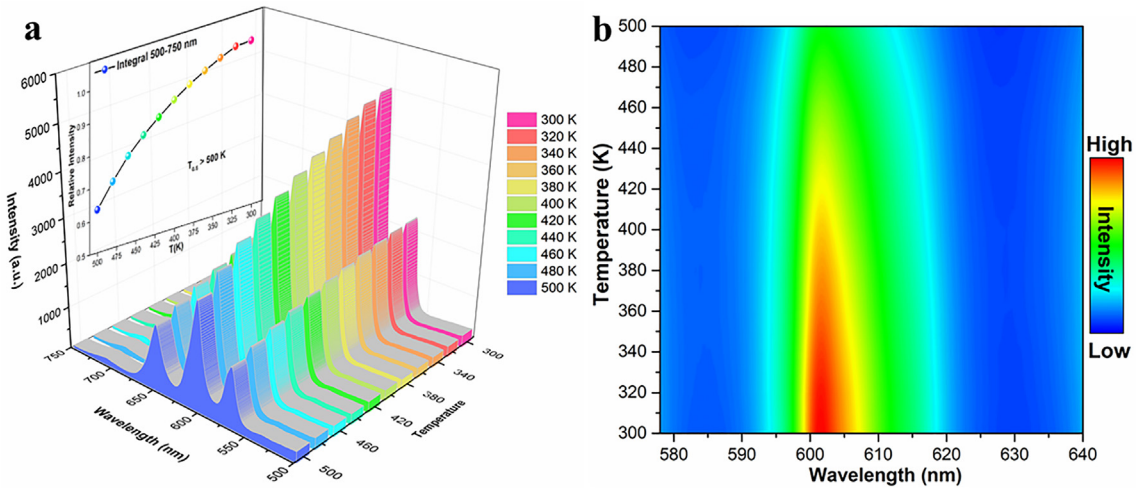

Fig. 10 (a) The PL spectra of LTWO:0.01Sm^{3+} detected from 300 to 500 K under 404 nm excitation. Iinset: The relationship between PL intensity and temperature). (b) The intensity of the strongest peak (597 nm) changing with temperature of LTWO:0.01Sm^{3+} phosphor.

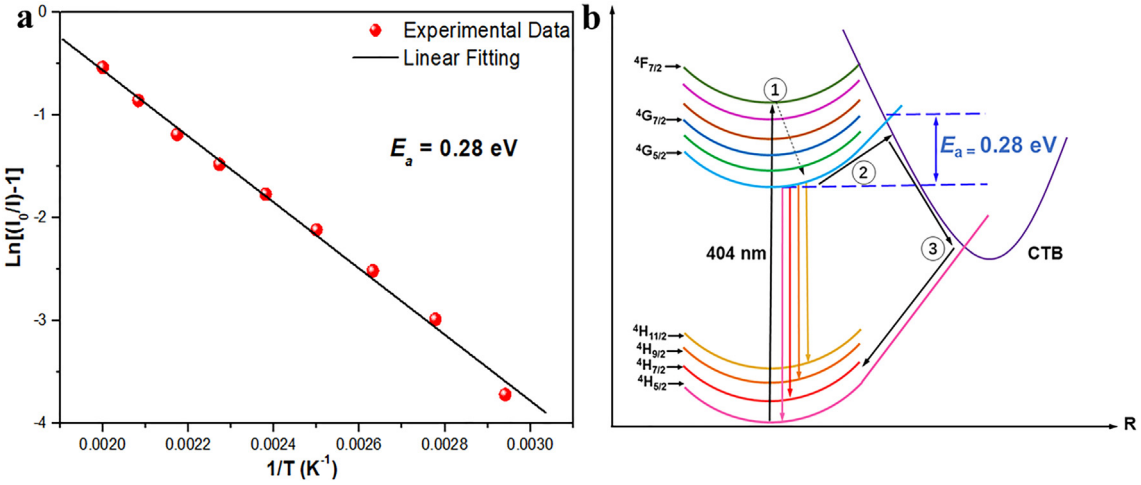

Fig. 11 (a) The activation energy photograph of LTWO:0.01Sm^{3+} phosphor for the thermal quenching process. (b) Thermal quenching mechanism of Sm^{3+} in LTWO host.

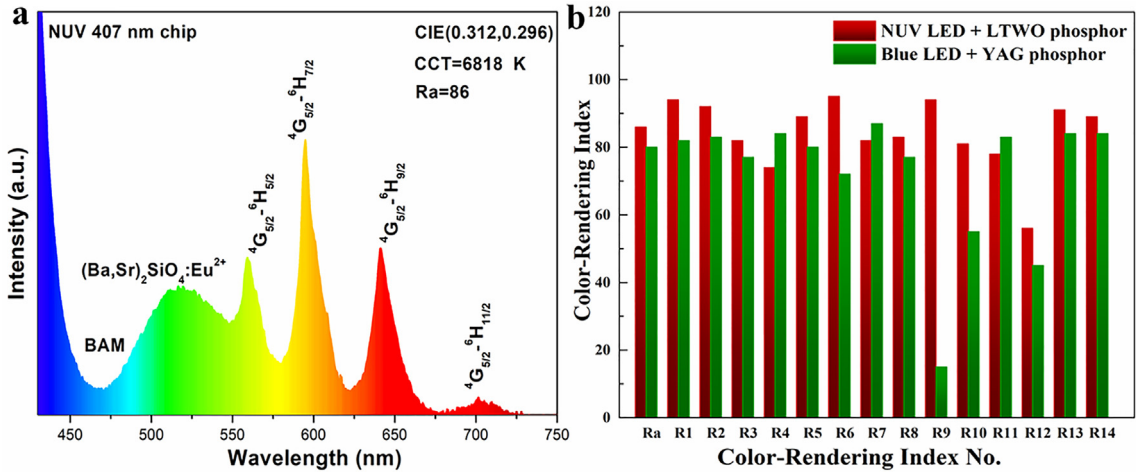

Fig. 12 (a) The EL spectrum of the w-LED fabricated by a NUV 407 nm chip with BAM, (Ba, Sr)$_2SiO_4:Eu^{2+}$ and LTWO:0.01Sm^{3+}. (b) The Ra histogram of the w-LED manufactured by combining NUV chip with LTWO:0.01Sm^{3+} phosphor and the commercial w-LED made by blue chip and YAG phosphor.

chip + YAG phosphor), it can be observed that the fabricated w-LED has higher Ra (86) and R9 (94) than Ra (80) and R9 (14) of the commercial w-LED (Zhang et al., 2008). These results indicate that the fabricated w-LED has stronger white light rendering performance than the commercial w-LED. The LTWO:Sm^{3+} phosphors can help to overcome the lack of red light in traditional commercial w-LEDs.

The CIE chromaticity coordinates and actual pictures of LTWO:0.01Sm^{3+} phosphor and the fabricated w-LED are shown in Fig. 13. The CIE chromaticity coordinates of LTWO:0.01Sm^{3+} are (0.590, 0.409), which fall in the orange-red region. The CIE chromaticity coordinates of the fabricated w-LED are (0.312, 0.296), which are in the centre of the white region. The real sample of LTWO:0.01Sm^{3+} phosphor emits bright orange-red light under the exposure of ultraviolet lamp. The fabricated w-LED shows a dazzling white light driven by a current of 300 mA and a voltage of 3.2 V. Therefore, all the results manifest that the LTWO:Sm^{3+} phosphors can be well applied in w-LEDs manufacture.

4. Conclusion

In summary, the novel orange-red light emitting LTWO:Sm^{3+} phosphors were successfully prepared via the solid-state reaction. The Rietveld refinement manifested that the samples belong to the trigonal crystal structure of space group *R*-3 (No.148), and Sm^{3+} ions replace La^{3+} ions in the LTWO lattice. The PLE spectrum demonstrates that the LTWO:Sm^{3+} phosphors can be availably excited by the O^{2-}-Sm^{3+} CTB, O^{2-}-W^{6+} CTB, and NUV light. The LTWO:Sm^{3+} phosphors emit intense orange-red light at 597 nm under 404 nm excitation, owing to the $^4G_{5/2}\rightarrow{}^6H_{7/2}$ transition. The quenching concentration of LTWO:Sm^{3+} phosphors is approximately 1 mol %. The main quenching mechanism of Sm^{3+} ions in LTWO

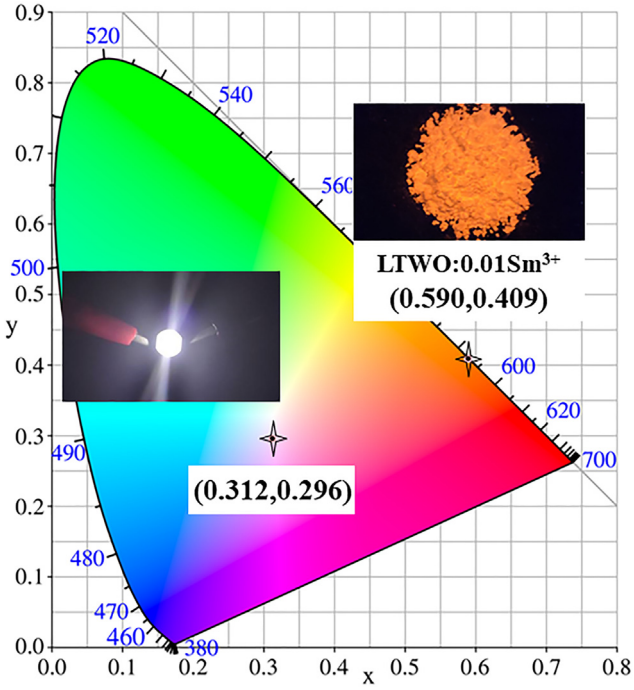

Fig. 13 The CIE chromaticity coordinates and actual pictures of LTWO:0.01Sm^{3+} phosphor and the fabricated w-LED.

host lattice is the dipole-dipole interaction. The quenching temperature is higher than 500 K, and the E_a is as high as 0.28 eV. By merging a NUV 407 nm chip with BAM blue phosphor, (Ba, Sr)$_2SiO_4$:Eu^{2+} green phosphor and LTWO:0.01Sm^{3+} orange-red phosphor, a w-LED with the CIE chromaticity coordinates of (0.312, 0.296) and Ra of 86 was obtained. All the results suggest that the orange-red LTWO:Sm^{3+} phosphors have the potential value to replace the commercial red phosphors in w-LEDs application.

Acknowledgments

The work was supported by the Natural Science Foundation of Shaanxi Province (Grant No. 2018JM5055), the Fundamental Research Funds for the Central Universities (2452019076), the Hunan Provincial Key Laboratory of Xiangnan Rare-Precious Metals Compounds and Applications (2019XGJSKFJJ01), the Construction Program of the key discipline in Hunan Province, the Projects of the Education Department of Hunan Province (No.18A465), the Science and Technology Plan Project of Chenzhou city (jsyf2017014) and Undergraduate Innovation Fund of Northwest A&F University, China (201910712037).

References

Al-Mamun, S.A., Ishigaki, T., 2014. Influence of hydrogen peroxide addition on photoluminescence of Y_2O_3:Eu^{3+} nanophosphors prepared by laser ablation in water. J. Am. Ceram. Soc. 97, 1083–1090.

Atuchin, V.V., Kesler, V.G., Maklakova, N.Y., Pokrovsky, L.D., 2005. Core level spectroscopy and RHEED analysis of KGd$(WO_4)_2$ surface. Solid State Commun. 133, 347–351.

Atuchin, V.V., Gavrilova, T.A., Grivel, J.C., Kesler, V.G., 2008. Electronic structure of layered titanate $Nd_2Ti_2O_7$. Surf. Sci. 602, 3095–3099.

Atuchin, V.V., Pokrovsky, L.D., Khyzhun, O.Y., Sinelnichenko, A.K., Ramana, C.V., 2008. Surface crystallography and electronic structure of potassium yttrium tungstate. J. Appl. Phys. 104. 033518.

Atuchin, V.V., Beisel, N.F., Galashov, E.N., Mandrik, E.M., Molokeev, M.S., Yelisseyev, A.P., Yusuf, A.A., Xia, Z., 2015. Pressure-stimulated synthesis and luminescence properties of microcrystalline (Lu, Y)$_3Al_5O_{12}$:Ce^{3+} garnet phosphors. ACS Appl. Mat. Interfaces 7, 26235–26243.

Atuchin, V.V., Aleksandrovsky, A., Chimitova, O., Diao, C.-P., Gavrilova, T., Kesler, V., Molokeev, M., Krylov, A., Bazarov, B., Bazarova, J., 2015. Electronic structure of β-RbSm $(MoO_4)_2$ and chemical bonding in molybdates. Dalton Trans. 44, 1805–1815.

Atuchin, V.V., Aleksandrovsky, A.S., Molokeev, M.S., Krylov, A.S., Oreshonkov, A.S., Zhou, D., 2017. Structural and spectroscopic properties of self-activated monoclinic molybdate $BaSm_2(MoO_4)_4$. J. Alloys Compd. 729, 843–849.

Cao, R., Chen, T., Ren, Y., Chen, T., Ao, H., Li, W., Zheng, G., 2019. Synthesis and photoluminescence properties of Ca_2LaTaO_6:Mn^{4+} phosphor for plant growth LEDs. J. Alloys Compd. 780, 749–755.

Chen, X., Lv, F., Ma, Y., Zhang, Y., 2016. Preparation and spectroscopic investigation of novel $NaAlP_2O_7$:Eu^{2+} phosphors for white LEDs. J. Alloys Compd. 680, 20–25.

Deng, H., Zhao, Z., Wang, J., Hei, Z., Li, M., Noh, H.M., Jeong, J.H., Yu, R., 2015. Photoluminescence properties of a new orange-red emitting Sm^{3+} doped $Y_2Mo_4O_{15}$ phosphor. J. Solid State Chem. 228, 110–116.

Deng, H., Gao, Z., Xue, N., Jeong, J.H., Yu, R., 2017. A novel Eu^{3+}-doped garnet-type tellurate red-emitting phosphor with high thermal stability and color purity. J. Lumin. 192, 684–689.

Devi, S., Dalal, M., Dalal, J., Hooda, A., Khatkar, A., Taxak, V.B., Khatkar, S.P., 2019. Near-ultraviolet excited down-conversion Sm^{3+}-doped $Ba_5Zn_4Gd_8O_{21}$ reddish-orange emitting nano-diametric rods for white LEDs. Ceram. Int. 45, 7397–7406.

Galashov, E.N., Atuchin, V.V., Gavrilova, T.A., Korolkov, I.V., Mandrik, Y.M., Yelisseyev, A.P., Xia, Z., 2017. Synthesis of $Y_3Al_5O_{12}$:Ce^{3+} phosphor in the Y_2O_3-Al metal-CeO_2 ternary system. J. Mater. Sci. 52, 13033–13039.

Goutenoire, F., Retoux, R., Suard, E., Lacorre, P., 1999. Ab Initiodetermination of the novel perovskite-related structure of $La_7Mo_7O_{30}$ from powder diffraction. J. Solid State Chem. 142, 228–235.

Goutenoire, F., Kodjikian, S., Suard, E., 2005. Extension of the $La_7Mo_7O_{30}$ structural type with $La_7Nb_3W_4O_{30}$ and $La_7Ta_3W_4O_{30}$ compounds. J. Solid State Chem. 178, 2811–2817.

Guo, C., Luan, L., Chen, C., Huang, D., Su, Q., 2008. Preparation of Y_2O_2S:Eu^{3+} phosphors by a novel decomposition method. Mater. Lett. 62, 600–602.

Guo, Q., Zhao, C., Liao, L., Lis, S., Liu, H., Mei, L., Jiang, Z., 2017. Luminescence investigations of novel orange-red fluorapatite $KLaSr_3(PO_4)_3F$:Sm^{3+} phosphors with high thermal stability. J. Am. Ceram. Soc. 100, 2221–2231.

Huang, X., Guo, H., 2018. $LiCa_3MgV_3O_{12}$:Sm^{3+}: A new high-efficiency white-emitting phosphor. Ceram. Int. 44, 10340–10344.

Huang, X., Wang, S., Li, B., Sun, Q., Guo, H., 2018. High-brightness and high-color purity red-emitting $Ca_3Lu(AlO)_3(BO_3)_4$:Eu^{3+} phosphors with internal quantum efficiency close to unity for near-ultraviolet-based white-light-emitting diodes. Opt. Lett. 43, 1307–1310.

Jaiswal, V.V., Bishnoi, S., Swati, G., Singh, P., Lohia, N., Bathula, S., Haranath, D., 2020. Luminescence properties of yttrium gadolinium orthovanadate nanophosphors and efficient energy transfer from VO_4^{3-} to Sm^{3+} via Gd^{3+} ions. Arab. J. Chem. 13, 474–480.

Ji, H., Huang, Z., Xia, Z., Molokeev, M.S., Atuchin, V.V., Fang, M., Huang, S., 2014. New yellow-emitting whitlockite-type structure

$Sr_{1.75}Ca_{1.25}(PO_4)_2:Eu^{2+}$ phosphor for near-UV pumped white light-emitting devices. Inorg. Chem. 53, 5129–5135.

Ji, H., Wang, L., Molokeev, M.S., Hirosaki, N., Xie, R., Huang, Z., Xia, Z., ten Kate, O.M., Liu, L., Atuchin, V.V., 2016. Structure evolution and photoluminescence of $Lu_3(Al, Mg)_2(Al, Si)_3O12:^{Ce}3+$ phosphors: new yellow-color converters for blue LED-driven solid state lighting. J. Mater. Chem. C 4, 6855–6863.

La7Ta3W4O30 Crystal Structure: Datasheet from "PAULING FILE Multinaries Edition – 2012" in SpringerMaterials (https://materials.springer.com/isp/crystallographic/docs/sd_1210382), in: P. Villars, K. Cenzual (Eds.), Springer-Verlag Berlin Heidelberg & Material Phases Data System (MPDS), Switzerland & National Institute for Materials Science (NIMS), Japan.

Lacorre, P., Corbel, G.l., 2019. Extension of the $A_nB_nO_{3n+2}$ slicing/oxidizing process from 2D layered to 1D columnar perovskites: the $La_7W_{7-x}M_xO_{30}$ structural family with Di-, Tri-, and tetravalent transition metal m substitutes to tungsten. Inorg. Chem. 58, 4289–4299.

Leaño Jr, J.L., Lin, S.-Y., Lazarowska, A., Mahlik, S., Grinberg, M., Liang, C., Zhou, W., Molokeev, M.S., Atuchin, V.V., Tsai, Y.-T., 2016. Green light-excitable Ce-doped nitridomagnesoaluminate Sr $[Mg_2Al_2N_4]$ phosphor for white light-emitting diodes. Chem. Mater. 28, 6822–6825.

Li, S., Liu, X., Mao, R., Huang, Z., Xie, R., 2015. Red-emission enhancement of the $CaAlSiN_3:Eu^{2+}$ phosphor by partial substitution for Ca_3N_2 by $CaCO_3$ and excess calcium source addition. RSC Adv. 5, 76507–76515.

Li, G., Wei, Y., Long, W., Xu, G., 2017. Photoluminescence properties, energy transfer and thermal stability of the novel red-emitting $CaGd_2(WO_4)_4:Eu^{3+}$, Sm^{3+} phosphors. Mater. Res. Bull. 95, 86–94.

Li, H., Yang, H.K., Moon, B.K., Choi, B.C., Jeong, J.H., Jang, K., Lee, H.S., Yi, S.S., 2011. Crystal structure, eectronic structure, and optical and photoluminescence properties of Eu(III) ion-doped $Lu_6Mo(W)O_{12}$. Inorg. Chem. 50, 12522–12530.

Liang, J., Devakumar, B., Sun, L., Sun, Q., Wang, S., Li, B., Chen, D., Huang, X., 2019. Mn^{4+}-activated $KLaMgWO_6$: A new high-efficiency far-red phosphor for indoor plant growth LEDs. Ceram. Int. 45, 4564–4569.

Lim, C.S., Aleksandrovsky, A., Molokeev, M., Oreshonkov, A., Atuchin, V., 2015. Microwave sol-gel synthesis and upconversion photoluminescence properties of $CaGd2(WO_4)_4:Er^{3+}/Yb^{3+}$ phosphors with incommensurately modulated structure. J. Solid State Chem. 228, 160–166.

Min, Q., Bian, W., Qi, Y., Lu, W., Yu, X., Xu, X., Zhou, D., Qiu, J., 2017. Temperature sensing based on the up-conversion emission of Tm^{3+} in a single $KLuF_4$ microcrystal. J. Alloys Compd. 728, 1037–1042.

Qiao, J., Zhang, Z., Zhao, J., Xia, Z., 2019. Tuning of the compositions and multiple activator sites toward single-phased white emission in $(Ca_{9-x}Sr_x)MgK(PO_4)_7:Eu^{2+}$ phosphors for solid-state lighting. Inorg. Chem. 58, 5006–5012.

Robertson, A.R., 1968. Computation of correlated color temperature and distribution temperature. J. Opt. Soc. Am. 58, 1528–1535.

Seeta Rama Raju, G., Park, J.Y., Jung, H.C., Pavitra, E., Moon, B.K., Jeong, J.H., Yu, J.S., Kim, J.H., Choi, H., 2011. Blue and green emissions with high color purity from nanocrystalline $Ca_2Gd_8Si_6O_{26}$:Ln (Ln = Tm or Er) phosphors. J. Alloys Compd. 509, 7537–7542.

Shannon, R.D., 1976. Revised effective ionic radii and systematic studies of interatomic distances in halides and chalcogenides. Acta Crystallographica Section A: Crystal Phys., Diffraction, Theoretical General Crystallography 32, 751–767.

Sun, Q., Wang, S., Devakumar, B., Li, B., Sun, L., Liang, J., Huang, X., 2018. Synthesis and photoluminescence properties of novel far-red-emitting $BaLaMgNbO_6:Mn^{4+}$ phosphors for plant growth LEDs. RSC Adv. 8, 28538–28545.

Tang, L., Gui, W., Ding, K., Chen, N., Du, G., 2014. Ion exchanged $YVO_4:Eu^{3+}$ nanocrystals and their strong luminescence enhanced by energy transfer of thenoyltrifluoroacetone ligands. J. Alloys Compd. 590, 277–282.

Tang, Y., Zhou, S., Yi, X., Zhang, S., Hao, D., Shao, X., 2017. The Cr-doping effect on white light emitting properties of Ce: YAG phosphor ceramics. J. Am. Ceram. Soc. 100, 2590–2595.

Tian, Y., Chen, B., Tian, B., Hua, R., Sun, J., Cheng, L., Zhong, H., Li, X., Zhang, J., Zheng, Y., Yu, T., Huang, L., Meng, Q., 2011. Concentration-dependent luminescence and energy transfer of flower-like $Y_2(MoO_4)_3:Dy^{3+}$ phosphor. J. Alloys Compd. 509, 6096–6101.

Tian, B., Chen, B., Tian, Y., Li, X., Zhang, J., Sun, J., Zhong, H., Cheng, L., Fu, S., Zhong, H., Wang, Y., Zhang, X., Xia, H., Hu, R., 2013. Excitation pathway and temperature dependent luminescence in color tunable $Ba_5Gd_8Zn_4O_{21}:Eu^{3+}$ phosphors. J. Mater. Chem. C 1, 2338–2344.

Trunov, V., Lykova, L., Afonskii, N., 1968. The structure of $Y_{0.33}TaO_3$ and $La_{0.33}TaO_3$. Khimiya 9, 55–58.

Wang, S., Song, Z., Kong, Y., Zhang, S., Xia, Z., Liu, Q., 2018. Enhanced performance of $Sr_2Si_5N_8:Eu^{2+}$ red afterglow phosphor by co-doping with boron and oxygen. J. Lumin. 204, 36–40.

Wang, C., Takeda, T., ten Kate, O.M., Tansho, M., Deguchi, K., Takahashi, K., Xie, R., Shimizu, T., Hirosaki, N., 2017. Ce-doped $La_3Si_{6.5}Al_{1.5}N_{9.5}O_{5.5}$, a rare highly efficient blue-emitting phosphor at short wavelength toward high color rendering white LED application. ACS Appl. Mat. Interfaces 9, 22665–22675.

Wang, S., Xu, Y., Chen, T., Jiang, W., Liu, J., Zhang, X., Jiang, W., Wang, L., 2019. A novel red phosphor $Ba_2La_4Y_4(SiO_4)_6O_2:Eu^{3+}$ with high quantum yield and thermal stability for warm white LEDs. J. Alloys Compd. 789, 381–391.

Xia, Z., Liu, R.-S., 2012. Tunable blue-green color emission and energy transfer of $Ca_2Al_3O_6F:Ce^{3+}$, $T^{b3}+$ phosphors for near-UV white LEDs. J. Phys. Chem. C 116, 15604–15609.

Xia, Z., Zhang, Y., Molokeev, M.S., Atuchin, V.V., 2013. Structural and luminescence properties of yellow-emitting $NaScSi_2O_6:Eu^{2+}$ phosphors:Eu^{2+} site preference analysis and generation of red emission by codoping Mn^{2+} for white-light-emitting diode applications. J. Phys. Chem. C 117, 20847–20854.

Xu, X., He, Q., Yan, L., 2013. White-light long persistent and photostimulated luminescence in $CaSnSiO_5:Dy^{3+}$. J. Alloys Compd. 574, 22–26.

Yu, R., Shin, D.S., Jang, K., Guo, Y., Noh, H.M., Moon, B.K., Choi, B.C., Jeong, J.H., Yi, S.S., 2014. Photoluminescence properties of novel Host-sensitized $Y_6WO_{12}:Dy^{3+}$ phosphors. J. Am. Ceram. Soc. 97, 2170–2176.

Yu, R., Xue, N., Wang, T., Zhao, Z., Wang, J., Hei, Z., Li, M., Noh, H.M., Jeong, J.H., 2015. Photoluminescence characteristics of high thermal stable fluorosilicate apatite $Ba_2Y_3(SiO_4)_3F:Sm^{3+}$ orange-red emitting phosphor. Ceram. Int. 41, 6030–6036.

Zhang, Y., Li, L., Zhang, X., Xi, Q., 2008. Temperature effects on photoluminescence of $YAG:Ce^{3+}$ phosphor and performance in white light-emitting diodes. J. Rare Earths 26, 446–449.

Zhang, Y., Ding, B., Yin, L., Xin, J., Zhao, R., Zheng, S., Yan, X., 2018. Monoclinic $Lu_{2-x}Sm_xWO_6$ based white light-emitting phosphors: from ground-excited-states calculation prediction to experiment realization. Inorg. Chem. 57, 507–518.

Zhang, Y., Chen, B., Xu, S., Li, X., Zhang, J., Sun, J., Zhang, X., Xia, H., Hua, R., 2018. A universal approach for calculating the Judd-Ofelt parameters of RE^{3+} in powdered phosphors and its application for the beta-$NaYF_4:Er^{3+}/Yb^{3+}$ phosphor derived from auto-combustion-assisted fluoridation. PCCP 20, 15876–15883.

Zhang, Z., Li, C., Han, C., Li, J., Jia, Y., Wang, D., 2016. High-brightness Sm^{3+} doped $La_{0.67}Mg_{0.5}W_{0.5}O_3$ red phosphor for NUV light-emitting diodes application. J. Alloys Compd. 654, 146–150.

Zhao, L., Meng, D., Li, Y., Zhang, Y., Wang, H., 2017. Tunable emitting phosphors $K_3Gd(PO_4)_2:Tm^{3+}$-Dy^{3+} for lightemitting diodes and field emission displays. J. Alloys Compd. 728, 564–570.

Zhao, L., Xu, P., Fan, F., Yu, J., Shang, Y., Li, Y., Huang, L., Yu, R., 2019. Synthesis and photoluminescence properties of Sm^{3+} and Dy^{3+} ions activated double perovskite Sr_2MgTeO_6 phosphors. J. Lumin. 207, 520–525.

Zou, J., Yang, B., Li, J., Zhu, S., Qian, X., Wang, F., 2016. Effect of Sr/Ca substitution on phase structure and photoluminescence properties of micro-$Sr_xCa_{1-x}AlSiN_3:Eu^{2+}$ phosphor for high CRI white LEDs. Ceram. Int. 42, 14956–14962.